Concurrent *AFG3L2* and *SPG7* mutations associated with syndromic parkinsonism and optic atrophy with aberrant OPA1 processing and mitochondrial network fragmentation

Stefania Magri,[1] Valentina Fracasso,[1] Massimo Plumari,[1,§] Enrico Alfei,[2] Daniele Ghezzi,[1,3] Cinzia Gellera,[1] Paola Rusmini,[4] Angelo Poletti,[4] Daniela Di Bella,[1] Antonio E. Elia,[5] Chiara Pantaleoni,[2] and Franco Taroni[1]*

[1]Unit of Medical Genetics and Neurogenetics, Fondazione IRCCS Istituto Neurologico Carlo Besta, Milan, Italy
[2]Unit of Developmental Neurology, Fondazione IRCCS Istituto Neurologico Carlo Besta, Milan, Italy
[3]Dipartimento di Fisiopatologia Medico-Chirurgica e dei Trapianti, Università degli Studi di Milano, Milan, Italy
[4]Dipartimento di Scienze Farmacologiche e Biomolecolari (DiSFeB), Centro di Eccellenza sulle Malattie Neurodegenerative, Università degli Studi di Milano, Milan, Italy
[5]Unit of Neurology 1, Fondazione IRCCS Istituto Neurologico Carlo Besta, Milan, Italy

[§]Present address: Genomic and Post-genomic Center, IRCCS Foundation "C. Mondino" National Neurological Institute, Pavia, Italy

*Corresponding author:
Franco Taroni, MD
Unit of Medical Genetics and Neurogenetics
Fondazione IRCCS Istituto Neurologico Carlo Besta
via Celoria 11
20133 Milan
Italy
email: *franco.taroni@istituto-besta.it*
Fax: +39-02-700548648

This article has been accepted for publication and undergone full peer review but has not been through the copyediting, typesetting, pagination and proofreading process, which may lead to differences between this version and the Version of Record. Please cite this article as doi: 10.1002/humu.23658.

FUNDING

This work was supported by grants from the Italian Ministry of Health (RF-2011-02351165), E-Rare (E-Rare-2 JTC 2011 EuroSCAR), and Fondazione Telethon (GGP09301) to F.T.

Abstract (200 words, max=200)

Mitochondrial dynamics and quality control are crucial for neuronal survival and their perturbation is a major cause of neurodegeneration. *m*-AAA complex is an ATP-dependent metalloprotease located in the inner mitochondrial membrane and involved in protein quality control. Mutations in the *m*-AAA subunits AFG3L2 and paraplegin are associated with autosomal dominant spinocerebellar ataxia (SCA28) and autosomal recessive hereditary spastic paraplegia (SPG7), respectively. We report a novel *m*-AAA-associated phenotype characterized by early-onset optic atrophy with spastic ataxia and L-Dopa-responsive parkinsonism. The proband carried a *de-novo AFG3L2* heterozygous mutation (p.R468C) along with a heterozygous maternally-inherited intragenic deletion of *SPG7*. Functional analysis in yeast demonstrated the pathogenic role of *AFG3L2* p.R468C mutation shedding light on its pathogenic mechanism. Analysis of patient's fibroblasts showed an abnormal processing pattern of OPA1, a dynamin-related protein essential for mitochondrial fusion and responsible for most cases of hereditary optic atrophy. Consistently, assessment of mitochondrial morphology revealed a severe fragmentation of the mitochondrial network, not observed in SCA28 and SPG7 patients' cells. This case suggests that coincidental mutations in both components of the mitochondrial *m*-AAA protease may result in a complex phenotype and reveals a crucial role for OPA1 processing in the pathogenesis of neurodegenerative disease caused by *m*-AAA defects.

KEYWORDS

AFG3L2

paraplegin

optic atrophy

parkinsonism

spastic ataxia

mitochondria

neurodegeneration

1. INTRODUCTION

The mitochondrial matrix AAA metalloprotease (*m*-AAA) is an ATP-dependent proteolytic complex located in the inner mitochondrial membrane (IMM), where it carries out protein quality control by degrading non-assembled or damaged proteins of the IMM and participates in the processing and maturation of some mitochondrial proteins (Esser et al., 2002; Nolden et al., 2005; Koppen & Langer, 2007). In humans, *m*-AAA exists in two different subunit compositions: a heterocomplex composed of AFG3L2 and paraplegin and a homocomplex constituted of AFG3L2 only. Interestingly, mutations in *AFG3L2* (MIM# 604581) cause an autosomal dominant form of spinocerebellar ataxia (SCA28, MIM# 610246) (Di Bella et al., 2010), while loss-of-function mutations in *SPG7* (encoding paraplegin, MIM# 602783) cause an autosomal recessive form of hereditary spastic paraplegia (SPG7, MIM# 607259) (Casari et al., 1998). Furthermore, homozygous hypomorphic *AFG3L2* mutations have been associated with a complex autosomal recessive spastic ataxia syndrome (SPAX5, MIM# 614487) (Pierson et al., 2011; Muona et al., 2015), while dominant mutations of SPG7 (Klebe

et al., 2012) and AFG3L2 (Charif et al., 2015) have been associated with nonsyndromic dominant optic atrophy (DOA).

We report here co-occurrence of a heterozygous *de-novo* AFG3L2 missense mutation (p.R468C) and a maternally-inherited heterozygous intragenic deletion of *SPG7* in a patient with a complex ataxic and extrapyramidal phenotype with early-onset optic atrophy. Interestingly, the *AFG3L2* p.R468C mutation was recently reported in a dominant family with optic atrophy and mild intellectual disability (Charif et al., 2015) and in a sporadic patient with isolated optic atrophy (Colavito et al., 2017). In neither case did the patients manifest ataxia, spasticity, or extrapyramidal involvement. Thus, the clinical and cellular studies described here suggest that co-occurrence of *AFG3L2* and *SPG7* mutations may result in a new complex phenotype not attributable to either of the two genes individually.

2. MATERIALS AND METHODS

2.1 Patient and DNA samples

All procedures involving human subjects were approved by the Institutional Review Board of the Fondazione IRCCS Istituto Neurologico “Carlo Besta”, Milan, Italy, in agreement with the Declaration of Helsinki. Each individual providing a biological sample signed written informed consent approved by the Institutional Review Board of the Foundation IRCCS Istituto Neurologico Carlo Besta, Milan, Italy, in agreement with the Declaration of Helsinki. Genomic DNA was prepared from peripheral-blood lymphocytes using standard procedures as previously described (Gellera et al., 2007).

2.2 Genetic studies

Mutation screening of *AFG3L2*, *SPG7*, and *OPA1* (MIM# 605290) genes was performed by Sanger sequencing, while copy number variation of *SPG7* was detected by MLPA (Multiplex Ligation-dependent Probe Amplification, MRC-Holland, Amsterdam, The Netherlands). Sequences of the oligonucleotide primers are available upon request. DNA mutation numbering system is based on cDNA sequence. Nucleotides are numbered so that the first nucleotide of the first in-frame ATG codon in the reference sequence is nucleotide +1. Amino acids are numbered so that methionine encoded by the first in-frame ATG codon in the reference sequence is Met1.

Segregation study was performed using a ultra-deep (≥20,000X) sequencing of PCR amplicons. NGS library was prepared from PCR amplicons using Nextera XT DNA Library Preparation Kit (Illumina, Inc., San Diego, CA, USA) according to the manufacturer's instructions and sequenced on a MiSeq sequencing apparatus (Illumina, Inc.) with high depth of coverage (>20,000-fold) for mosaicism detection.

Paternity testing was performed using multiallelic variable number of tandem repeat (VNTR) polymorphisms 3'APOB-VNTR (Deka et al., 1992) and D11S533 (Eubanks et al., 1991).

Sequencing of 4,813 genes associated with known clinical phenotypes was performed using TruSight One sequencing panel kit (Illumina, Inc.; www.illumina.com/trusightone) on an Illumina MiSeq sequencer according to the manufacturer's instructions. Data analysis was performed using: a) MiSeq Reporter software (Illumina, Inc.) for alignment and variant calling; b) VariantStudio software (Illumina, Inc.) for variant annotation; and c) CLC Genomics Workbench (CLCbio-Qiagen, Aarhus, Denmark) software for quality control and

coverage analysis. Filtering passing variants were classified and prioritized according to the ACMG Standards and Guidelines (Richards et al., 2015). Potentially pathogenic variants in genes associated with optic atrophy, dystonia, spastic paraplegia, ataxia, or Parkinson disease (Supp. Tables S1 and S2) were confirmed in the proband by Sanger sequencing and segregated in her parents by Illumina Nextera XT deep sequencing.

2.3 AFG3L2 and paraplegin yeast expression plasmids

Plasmids for heterologous expression of human AFG3L2 and paraplegin in yeast were generated as previously described (Di Bella et al., 2010). Mutations were introduced into the yeast construct pYC6/CT*ADH1*-AFG3L2-V5/HIS using the QuikChange XL Site-Directed Mutagenesis Kit (Stratagene-Agilent, Cedar Creek, TX, USA). All AFG3L2 forms were C-ter tagged with the V5 epitope (amino acid residues 95-108, GKPIPNPLLGLDST, of RNA polymerase alpha subunit of simian virus 5). Sequences of oligonucleotide primers used for site-directed mutagenesis are available upon request. Plasmid pYC2/CT-*ADH1*-AFG3L2-myc carrying wild-type AFG3L2 was used to express AFG3L2^{mut}/AFG3L2^{wt} complex as previously described (Di Bella et al., 2010). Plasmid YCplac111*ADH1*-Yta10(1-63)-paraplegin(59-795)-HA was used to express human paraplegin as previously described (Di Bella et al., 2010).

2.4 Yeast strains and growth conditions

All strains used in this study (Supp. Table S3) derived from W303 (K699, *MATa ho ade2-1 trp1-1 can1-100 leu2-3,12 his3-11,15 ura3 ssd1*). A double-knockout yeast strain (*yta10Δyta12Δ*) was generated by deleting *YTA10* and *YTA12,* the yeast orthologs of human AFG3L2 and paraplegin, respectively, using the one-step PCR system; the obtained strain

was transformed as previously described (Di Bella et al., 2010). Cells were grown at 28°C on YEP medium (1%-yeast extract, 2%-peptone, 2%-agar for plates) or selective medium supplemented with 2% (wt/vol) glucose according to standard procedures. Blasticidin-resistant transformants were selected on YEP medium supplemented with 50 µg of blasticidin S per ml. For complementation experiments, equal amounts of five-fold serial dilutions of cells from exponentially grown cultures were spotted onto YEP plates containing 2% (wt/vol) glucose (YPD) or 2% (wt/vol) glycerol (YPG) and incubated at 28°C or 37°C, as indicated. For growth rate analysis, we precultured overnight yeast cells in selective medium supplemented with 2% (wt/vol) galactose and 0.1% (wt/vol) glucose and then cultured them in YEP medium supplemented with 2% (wt/vol) glycerol for 24 h, inoculated at a standard density of approximately 1×10^6 cells/ml. We removed samples at 0h, 20h and 24h and determined cell density spectrophotometrically, expressed as OD_{600}. For western blot analysis, yeast cells were cultured overnight in selective medium supplemented with 2% (wt/vol) galactose and 0.1% (wt/vol) glucose and normalized spectrophotometrically at OD_{600}.

2.5 Immunoblot analysis and antibodies

For western blot analysis of yeast cells, trichloroacetic acid (TCA) protein extracts were prepared as described (Muzi-Falconi et al., 1993). Western blot analysis of COX subunits was performed on mitochondrial extracts. Protein extracts were separated by SDS-PAGE in 10% or 15% acrylamide gels as indicated and transferred to a PVDF membrane (Immobilon LF, EMD Millipore/Fisher Scientific, Hampton, NH, USA). Filters were probed with antibodies (Supp. Table S4) as indicated in the text and in the figure legends. Fluorescent blot was performed using Alexa Fluor®647-conjugated goat anti-rabbit IgG (H+L) antibody

and Alexa Fluor®488-conjugated goat anti-mouse IgG (H+L) antibody (Invitrogen Molecular Probes/Thermo Fisher Scientific Inc., Waltham, MA, USA). Fluorescence signals were acquired using the G:BOX iChemi apparatus (Syngene, Cambridge, UK); quantitation was performed using Gene Tools software (Syngene) on four independent western blots normalizing signals to the β-actin loading control. For western blot analysis of patient-derived lymphoblasts and fibroblasts, cell lysates from each line were electrophoresed on 10%-15%-SDS-polyacrylamide gels and transferred to a nitrocellulose membrane (Amersham Biosciences/GE Healthcare Life Sciences, Little Chalfont, UK) by electroblotting. Filters were probed with indicated antibodies and developed by HRP-conjugated secondary antibodies using a chemiluminescent substrate (ECL Prime, Amersham Biosciences). Signals were detected by G:BOX iChemi (Syngene). Quantitative analysis of OPA1 forms levels was performed using Gene Tools software (Syngene) on three independent immunoblots normalizing the signals to that of the alpha subunit of mitochondrial trifunctional protein (MTPα) as the loading control.

2.6 Assays of respiratory chain complexes activity

For *in vitro* activity assay of Complex III, IV, and V and immunoblot analysis of cytochrome *c* oxidase (COX) subunits, yeast cells were grown at 28°C in YEP medium supplemented with 2% (wt/vol) galactose-0.1% (wt/vol) glucose. Yeast cell mitochondria were prepared by differential centrifugations. The resulting mitochondrial pellet was resuspended in 10-mM potassium phosphate buffer and freezed and thawed for three times. Protein concentration was determined by Bradford microplate microassay (Bio-Rad Laboratories, Hercules, CA, USA) with bovine serum albumin as the standard. Respiratory chain enzyme activities were

determined spectrophotometrically as previously described (Di Bella et al., 2010; Magri et al., 2010). Activity was expressed as nanomoles per minute per milligram of protein.

2.7 Co-immunoprecipitation of AFG3L2 and paraplegin

For immunoprecipitation experiments, yeast cells were precultured overnight in a selective medium and then grown in 100 ml of YPD medium until 1x 10^7 cell/ml as previously described (Fracasso, 2010). Normalized cells were resuspended in PBS, 1 mM PMSF, 1 mM NaVa, 50 mM NaF supplemented with Complete Protease Inhibitor Cocktail (Hoffmann-La Roche, Basel, CH), and homogenized using the FastPrep® System (Qbiogene-MP Biomedicals). Homogenates were centrifuged and the resulting supernatants were incubated with anti-V5 antibodies (Invitrogen/Thermo Fisher Scientific Inc., Waltham, MA, USA). Antigen-antibody complexes were then incubated with Protein G Mag Sepharose (GE Healthcare Life Sciences, Little Chalfont, UK). Samples were eluted from beads and analysed by SDS-PAGE and immunoblotting.

2.8 Patient-derived cell lines

Epstein-Barr-virus-stabilized lymphoblastoid cell lines (LCL) from patients, their relatives and control subjects were established and cultured as previously described (Gellera et al., 2007). Fibroblasts from patient and controls were grown in the DMEM-high glucose or -galactose media as described previously (Wong et al., 1999).

2.9 Analysis of mitochondrial morphology

For analysis of mitochondrial morphology, fibroblasts were grown on coverslips inside a petri dish filled with the appropriate culture medium. When reached the desired confluence,

cells were incubated for 15 minutes with a medium containing 50-nM MitoTracker Red™ (Invitrogen Molecular Probes/Thermo Fisher Scientific Inc., Waltham, MA, USA). Stained cells were fixed using a 1:1 solution of 4% (w/v) saccharose and 4% (v/v) paraformaldeyde for 25 min at 37°C under weak agitation, and then in ice-cold methanol for 10 min at room temperature. Samples were analyzed with a Leica TCS NT confocal laser scanning microscope (Leica Lasertecknik GmbH, Heidelberg, Germany) equipped with a 75 mW Kripton/Argon mixed gas laser (Fig. 4B) or a Nikon Eclipse T1 fluorescent microscope with a oil objective (Supp. Fig. S9).

For quantitative analysis of mitochondrial network morphology, acquired images of mitochondria were analyzed using NIH-developed Image J software (Wayne Rasband, NIH, Bethesda, MD, USA). Raw images were first enhanced by 2D deconvolution (Iterative Deconvolve 3D by Robert Dougherty, OptiNav, Inc., Bellevue, WA, USA) and then converted into binary (black and white) images. Mitochondrial particles were analyzed determining, for each object, several parameters such as area (Am), perimeter (Pm), maximal and minimal radius. We used Aspect Ratio (AR) and Formfactor (F) as quantitative descriptors of mitochondrial morphology. Aspect Ratio is the ratio between the major and minor axis of the ellipse equivalent to the mitochondrion and reports changes in length, whereas Formfactor (defined as [Pm2]/[4πAm]) allows to quantify the degree of branching (Koopman et al., 2006). Both parameters are independent from image magnification and have a minimal value of 1, corresponding to a circular mitochondrion. Higher values of AR and F correspond to longer and more branching mitochondria, respectively. The results are shown in the bar graphs in Fig. 4C, which represent average AR and F values calculated on at least four randomly selected cells cultured in glucose- or galactose-containing medium as indicated.

2.10 Gene expression analysis

Total RNA was isolated from fibroblast cell lines derived from the affected patient and 4 controls with Maxwell® 16 LEV simplyRNA Cell Kit, according to the manufacturer's instructions (Promega Corporation, WI, USA). The quality and quantity of RNA were determined with a NanoDrop 2000 Spectrophotometer (Thermo Fisher Scientific Inc., Waltham, MA, USA). One microgram of total RNA was reverse-transcribed using the SuperScript® VILO™ cDNA Synthesis Kit according to the manufacturer's instructions (Thermo Fisher Scientific Inc., Waltham, MA USA).

Gene expression analysis was performed by TaqMan real-time PCR (RT-PCR) using the following TaqMan® Assays (Thermo Fisher Scientific Inc., Waltham, MA, USA): OMA1 (Hs00377028_m1), OPA1 (Hs01047013_m1), GAPDH (Hs02758991_g1). Expression levels of *OMA1 (MIM# 617081)*, *OPA1*, and *GAPDH* were determined using the Applied Biosystem Real Time-PCR 7300 system (Thermo Fisher Scientific Inc., MA, USA) following the manufacturer's instructions. Real-time PCR reaction was carried out in a final volume of 20 µl using 10 µl TaqMan® Fast Advanced Master Mix, 1-µl TaqMan® Gene Expression Assays and 1 µl cDNA sample with a pre-incubation step at 50°C for 2 minutes and at 95°C for 20 seconds, followed by 40 cycles at 95°C for 3 seconds, 60°C for 30 seconds. RT-PCR reactions were run in duplicate in each assay. The expression levels of *OMA1* and *OPA1*, first normalized to the expression levels of the housekeeping gene *GAPDH*, were further normalized for both patient and controls to the expression levels of a control individual used as calibrator. The experiments were performed in triplicate.

3 RESULTS

3.1 Case report

The proband is a 25-year-old woman with negative family history. She has nonconsanguineous healthy parents and two unaffected twin brothers (Fig. 1A). The disease presented at the age of 5 years with severe visual impairment (bilateral 1/20 visual acuity) and signs of primary optic atrophy: reduction of optic disc size with mild diffuse pallor, wedge-shaped area of excavation of the temporal sector, normal retinal blood vessels. At the age of 6 years, the patient manifested a slowly progressive motor impairment characterized by bradykinesia, internal rotation of right foot, and gait and balance instability. At 10 years, brain magnetic resonance imaging (MRI), visual evoked potentials, electroretinogram, nerve conduction studies, motor and sensory evoked potentials, and electroencephalogram (EEG) were normal. Neuropsychological studies showed mild cognitive impairment (WISC-R IQ=62) with relative preservation of verbal abilities (V=76, P=50). Since 12 years, she also exhibited spastic paraparesis with mild ataxia, scanning speech and mild drooling. At 14 years of age, L-dopa treatment (levodopa+carbidopa, 375+37.5 mg/die) was started, with significant improvement in gait function and global motility, but no effect on visual impairment. At 22 years of age, single photon emission computed tomography (SPECT)/dopamine transporter (DaT) scan showed marked bilateral dopaminergic defect in the striatum (Fig. 1B). Analysis of muscle biopsy showed normal muscle morphology, a mild reduction of complex I activity (10 nmol/min per mg protein; n.v., 13-24), and normal levels of Coenzyme Q_{10} and respiratory chain complexes II-V. At the age of 22 years, she experienced motor fluctuations characterized by “wearing-off” with lower limb painful

dystonia and peak-dose dyskinesias with facial grimaces and cervical dystonic movements. At last examination (25 years), she had spastic-ataxia combined with rigid akinetic parkinsonism with right side prevalence (UPDRS motor score: 5/108 in "on" state, 25/108 in "off" state). She exhibited good control of motor fluctuations after introduction of 4 mg/die rotigotine in association with levodopa+carbidopa (125+12.5 mg t.i.d.). Remarkably, brain MRI was still normal (Supp. Fig. S1). Optical coherent tomography (OCT) showed marked bilateral thinning of retinal fiber layer (RNFL) and ganglion cell layer (GCL) (Supp. Fig. S2). Cognitive evaluation (WISC-IV) confirmed discrepancy between verbal (VCI=73) and visual perceptual and speed processing skills (PRI=48, PSI=53), with mild working memory deficit (WMI=63).

3.2 Genetic analysis

Molecular screening for mitochondrial DNA Leber's hereditary optic neuropathy (LHON, MIM# 535000) mutations (m.3460G>A, m.11778G>A, m.14459G>A, and m.14484T>C), and mutations in the *OPA1* (MIM# 165500) (sequence and MLPA analysis) and *GCH1* (DYT5, MIM# 128230) genes resulted negative for pathogenic or likely pathogenic variants, while molecular analysis of *AFG3L2* revealed a previously reported (Charif et al., 2015) heterozygous missense variant p.R468C (NM_006796.2:c.1402C>T, submitted to ClinVar (https://www.ncbi.nlm.nih.gov/clinvar/)) (Fig. 1A) in the highly conserved SRH region of the ATPase domain. Both parents and the twin brothers were negative for the mutation and mosaicism was excluded by deep sequencing (>20,000X) analysis of parents' DNA (Supp. Fig. S3C), thus indicating the *de-novo* nature of the p.R468C mutation in this family. Because of its functional and genetic interaction with *AFG3L2*, we screened *SPG7* for mutations and identified a novel heterozygous deletion spanning exons 4 to 6

(NM_003119.3:c.(376+1_377-1)_(861+1_862-1)del, submitted to ClinVar) and predicted to cause premature termination of protein translation (p.Glu127SerfsTer2). The patient's mother and the twin brothers, who carried only the *SPG7* deletion, were completely unaffected, consistently with the recessive nature of SPG7 disease (Fig. 1A). Clinical exome analysis using Illumina TruSight One sequencing panel excluded the presence of pathogenic or likely pathogenic variants in other disease genes associated with optic atrophy, dystonia, spastic paraplegia, ataxia, or Parkinson disease (Supp. Tables S1 and S2). Finally, Southern blot analysis showed normal amount of normal-sized mtDNA with no evidence of deletions.

3.3 Functional analysis of AFG3L2 p.R468C variant in yeast

The functional consequences of AFG3L2 p.R468C variant were assessed using the yeast model we previously described (Di Bella et al., 2010). Human AFG3L2 protein carrying the p.R468C variant or two reference SCA28 pathogenic mutations (p.E691K, paraplegin-nonresponsive, and p.S674L, paraplegin-responsive (Di Bella et al., 2010)) was expressed in a *m*-AAA–defective strain (*yta10*Δ*yta12*Δ double-knockout strain) with and without paraplegin. Yeast cells lacking the endogenous *m*-AAA protease exhibit a respiratory defect (OXPHOS phenotype) which is complemented by wild-type AFG3L2 ($AFG3L2^{WT}$) but not by $AFG3L2^{R468C}$, indicating that this substitution is deleterious for homocomplex function (Fig. 2A). *yta10*Δ*yta12*Δ cells carrying $AFG3L2^{R468C}$/paraplegin also show an OXPHOS phenotype, indicating that the p.R468C mutation is not rescued by paraplegin (Fig. 2B). Furthermore, co-expression of $AFG3L2^{WT}$ in cells carrying $AFG3L2^{R468C}$ resulted in a very limited recovery of respiration (Supp. Fig. S4A) and in a persistent deficiency of both proteolytic and dislocase (ATPase) activities (Supp. Fig. S4B and C, respectively). Altogether, these experiments demonstrate the pathogenicity of the p.R468C variant and

suggest that it functionally inactivates both homo- and heterocomplex likely via a dominant-negative mechanism (Veitia et al., 2018).

Enzyme activity assay of respiratory chain complexes III, IV, and V in AFG3L2^{R468C} cells showed a reduction of >80% as compared to AFG3L2^{WT} (Fig. 2C). Notably, in comparison with the SCA28 mutations, the p.R468C is associated with a more severe cytochrome *c* oxidase (Cox) reduction (>90%) that persisted unchanged upon coexpression of paraplegin, consistent with the dominant effect of this mutation. Immunoblot protein level quantitation showed a severe reduction of both mitochondria-encoded Cox subunits (Cox1p, Cox2p, and Cox3p) and nucleus-encoded subunit Cox4p indicating a general downregulation of the whole enzyme (Supp. Fig. S5).

We also evaluated residual activity of human mutated *m*-AAA complexes, measuring the processing of the two known substrates of yeast *m*-AAA: the ROS-scavenger protein Ccp1 (Esser et al., 2002) and the ribosomal subunit MrpL32 (Nolden et al., 2005). In particular, the conversion of MrpL32 from precursor to mature form is an indicator of the overall proteolytic competence, while the maturation of Ccp1 indicates the ATP-dependent capacity of *m*-AAA complex to dislocate proteins from the IMM (dislocase activity) (Tatsuta et al., 2007; Bonn et al., 2011). Quantitation of protein precursor and mature levels showed that in yeast strains harbouring AFG3L2^{R468C}, both alone or with paraplegin, approx. 90% of MrpL32 and Ccp1 accumulate as precursor (Fig. 3A-B), indicating that the p.R468C mutation disrupts both proteolytic and ATPase (dislocase) activity.

Remarkably, the severity of the AFG3L2 p.R468C mutation is also demonstrated by the impairment of its own maturation that physiologically occurs by autocatalytic processing (Koppen et al., 2009). We performed immunoblot analysis of strains expressing homocomplex carrying the disease-causing mutation p.R468C, the reference SCA28

mutations p.E691K and p.S674L (Di Bella et al., 2010), and the proteolytically inactive mutant p.E575Q (Koppen et al., 2009) (Fig. 3C). This latter mutant accumulates as a larger form (p, precursor) (Fig. 3C and Supp. Fig. S6A, lane 6), indicating that human AFG3L2 undergoes autocatalytic processing as do the homolog mouse subunits Afg3l2 and Afg3l1 (Koppen et al., 2009). Unlike the SCA28 mutants, AFG3L2^{R468C} accumulates also as precursor protein (Fig. 3C and Supp. Fig. S6A, lane 3), indicating that this mutation impairs AFG3L2 maturation. Notably, in strain expressing AFG3L2^{R468C} and paraplegin, both proteins are almost completely unprocessed (Fig. 3D and Supp. Fig. S6B, lane 3), indicating a more severe impairment of the heterocomplex than the homocomplex. These results may reflect the different functional organization of the homo- and heterocomplex and the specific role of arginine 468 in intersubunit communication acting as a sensor of ATP in the neighbour subunit (Ogura et al., 2004). Coordinated ATP hydrolysis within the AAA ring of *m*-AAA proteases has been proposed to increase the efficiency of the proteolytic machine (Augustin et al., 2009), likely by inducing conformational changes necessary for protease functioning (Suno et al., 2006). It is conceivable that the dynamic motion of the subunits may differ between the homo- and heterocomplex, making the latter more vulnerable to the presence of a mutation in the crucial ATP sensor 468 residue.

To investigate the ability of AFG3L2^{R468C} to assemble in a heterocomplex, we performed co-immunoprecipitation in strains co-expressing paraplegin and AFG3L2^{WT} or AFG3L2^{R468C} (Supp. Fig. S7), which showed that AFG3L2^{R468C} is able to interact with paraplegin in its precursor form (lane 6).

Altogether, co-expression studies, substrate processing experiments, and co-immunoprecipitation results demonstrate that AFG3L2^{R468C} mutant can assemble into both

homomeric (AFG3L2/AFG3L2) and heteromeric (AFG3L2/paraplegin) complexes which are substantially inactive.

3.4 Functional analysis in patient's cells

To investigate the effect of *m*-AAA impairment on human cellular phenotype, we studied fibroblasts and lymphoblastoid cell lines (LCL) derived from the patient and controls. First, immunoquantitation in the patient's cells showed normal levels of AFG3L2 but reduced levels of paraplegin, consistent with heterozygosity for the SPG7 null mutation (Supp Fig. S8A). We then analysed the processing pattern of MRPL32 and OPA1, a dynamin-related protein crucial for mitochondrial dynamics and *cristae* morphogenesis, and responsible for most cases of dominant optic atrophy (MacVicar & Langer, 2016). Although both MRPL32 and *m*-AAA are highly conserved in eukaryotes, their interaction is not clearly demonstrated in mammals (Nolden et al., 2005; Maltecca et al., 2008). As previously observed in SCA28 patients' cells (Di Bella et al., 2010), immunoblot analysis revealed normal processing of MRPL32 in patient's fibroblasts cultured in both glucose and galactose (Supp. Fig. S8B). On the contrary, unlike what observed in SCA28 patients' cells (Di Bella et al., 2010), OPA1 presented an abnormal processing pattern (Fig. 4A). In particular, we observed a reduction of the long form L2 and the short form S2, and an accumulation of the S3 form. The same OPA1 pattern alteration was observed also in patient's LCLs (Supp. Fig. S8A).

Since under various stress conditions (loss of membrane potential, heat stress, reduction of ATP level, Bax/Bak aggregation, and other mitochondrial stress conditions) the cleavage of OPA1 long forms is enhanced by the overactivation of OMA1, an inducible ATP-independent metalloprotease of the inner mitochondrial membrane (Quirós et al., 2012; Baker et al., 2014), we investigated whether an increase in OMA1 mRNA could be

implicated in the aberrant processing pattern of OPA1 observed in the patient's cells (Supp. Fig. S10). We did not detect any statistically significant difference between OMA1 mRNA levels in patient's and controls' cells, which indicates that OMA1 increased activity, if any, is not mediated by transcriptional activation.

Since a balance of short and long OPA1 forms is required for mitochondrial fusion activity in mammals (Song et al., 2007), we investigated the morphology of the mitochondrial network. Analysis by confocal microscopy revealed a significant fragmentation in patient's fibroblasts as compared to control cells (Fig. 4B-C). Consistently, analysis of aspect ratio and formfactor (Koopman et al., 2006), which describe mitochondrial shape (length) and branching, respectively, showed significantly lower values in patient's cells than in control cells (Fig. 4C). However, despite this mitochondrial fragmentation, oxygen consumption rate (OCR, determined using Seahorse Bioscience XF Cell Mito Stress Test) was similar in patient's and controls' fibroblasts (data not shown). Notably, this is consistent with the recent observation that energetic competence of the cell may be independent of mitochondrial network morphology (Del Dotto et al., 2017).

4 DISCUSSION

In the present study, we describe for the first time a patient carrying heterozygous mutations in the *AFG3L2* and *SPG7* genes that encode the subunits of the mitochondrial *m*-AAA protease: *AFG3L2:*p.R468C (*de novo*) and *SPG7:*p.Glu127SerfsTer2 (maternally-inherited). This genotype is associated with a severe complex phenotype characterized by early-onset optic atrophy, L-dopa-responsive syndromic parkinsonism with abnormal dopaminergic uptake in the basal ganglia on SPECT/DaTscan (Fig. 1B), spastic ataxia, and mild cognitive

impairment. An extensive sequence analysis of the known genes causing optic atrophy, Parkinson disease, and hereditary dystonia allowed to exclude other molecular causes for the observed phenotype. Interestingly, the *AFG3L2* mutation p.R468C was recently described in a family with dominant optic atrophy and mild intellectual disability without any sign of ataxia, spasticity or extrapyramidal involvement (Charif et al., 2015) and in a sporadic patient with isolated optic atrophy (Colavito et al., 2017). While it was dominantly inherited in the first family, its transmission pattern could not be established in the second case. Interestingly, the *de-novo* nature of the mutation in our patient (Fig. 1A and Supp. Fig. S3) clearly indicates that *AFG3L2* NM_006796.2:c.1402C is a mutational hotspot.

The phenotype-genotype comparison between our *AFG3L2*/*SPG7* patient and the patients with *AFG3L2* p.R468C only (Charif et al., 2015; Colavito et al., 2017) suggests that the early-onset optic atrophy phenotype is due to this particular *AFG3L2* mutation, whose effects are greatly aggravated in our patient by the concurrent defect of paraplegin. Unlike *AFG3L2* mutations causing SCA28, which predominantly affect the proteolytic domain (Cagnoli et al., 2010; Di Bella et al., 2010), the p.R468C mutation involves a highly conserved arginine of the SRH region of the ATPase domain. The corresponding arginine of various AAA/AAA+ ATPases is essential for ATP hydrolysis because it acts as a sensor for the presence of ATP in the neighbour subunit interacting with the ATP γ-phosphate in the ATP-binding pocket of the adjacent subunit (Ogura et al., 2004). Thus, this residue represents the arginine finger which contributes to the coupling of the free energy of ATP hydrolysis to the conformational changes necessary to drive the translocation of a substrate polypeptide to the protease catalytic sites (Suno et al., 2006). Consistently, functional analysis in our yeast model demonstrated that p.R468C completely abolished both the ATPase-dependent dislocase activity, essential for the processing of membrane proteins (Fig. 3B), and the

proteolytic competence (Fig. 3A). Interestingly, we demonstrated that in yeast AFG3L2^{R468C} retains the ability to assemble in complexes (Supp. Fig. S7) but is unable to support its autoprocessing and the proteolytic activation of paraplegin (Fig. 3C and D), which would indicate that the complex is inactive. By contrast, the SCA28 mutations (p.E691K and p.S674L (Di Bella et al., 2010)), that affect the proteolytic domain, not only modestly alter the ATP-dependent dislocase activity (these AFG3L2 mutants are able to process Ccp1 almost as AFG3L2^{WT} does (Fig. 3B)), but also show a residual proteolytic activity (Fig. 3A, C, and D), which would indicate the formation of partially active complexes. The peculiar molecular pathomechanism of the AFG3L2$^{p.R468C}$ mutation may therefore account for the different patient phenotypes (i.e., SCA28 *vs.* DOA)..

Remarkably, our proband exhibits a complex phenotype that is very likely caused by the synergistic effect of a dominant-negative *AFG3L2* mutation and the reduced levels of paraplegin due to a loss-of-function *SPG7* mutation. The genetic interaction between *AFG3L2* and *SPG7* was demonstrated in mice, where the double mutants *Spg7*$^{-/-}$*Afg3l2*$^{Emv66/+}$ show an early-onset severe neurological phenotype that represents an acceleration and worsening of the phenotype observed in single mutants (Martinelli et al., 2009). Haploinsufficient *Afg3l2*$^{Emv66/+}$ mice appear normal at birth and do not show a remarkable phenotype up to 4 months of age when they develop a slowly progressive motor coordination deficit (Maltecca et al., 2009). By contrast, crossing these mice with paraplegin-deficient mice (*Spg7*$^{-/-}$*Afg3l2*$^{Emv66/+}$ double mutants) resulted in a severe neurological phenotype manifesting at 6 weeks of age, characterized by reduced cage activity, loss of balance, and frank uncoordinated gait with dystonic movements of the head by 9 weeks of age. Later, they lost significant weight, became cachexic, and eventually died within the 4th month of life (Martinelli et al., 2009). Therefore, these mice displayed an acceleration of the features of

paraplegin-deficient mice (Ferreirinha et al., 2004), showing axonal degeneration in the spinal cord much earlier (13 weeks *vs*. 8 months) than in the sole absence of Spg7. Altogether, these findings suggest that neurons are very sensitive to the global levels and the subunit composition of *m*-AAA proteases and lend support to the hypothesis that digenic inheritance of *AFG3L2* and *SPG7* mutations may result in more complex phenotype(s) not attributable to either of the two genes individually.

Another striking difference from SCA28 patients (Cagnoli et al., 2006; Di Bella et al., 2010) was the clear evidence of systemic mitochondrial involvement in this patient. First, muscle biopsy revealed an isolated Complex I deficiency; second, patient's cells presented an altered OPA1 pattern and mitochondrial network fragmentation (Fig. 4 and Supp. Fig. S8 and S9). Interestingly, syndromic and nonsyndromic Parkinson disease was recently observed in some patients carrying missense mutations in the *OPA1* gene (Carelli et al., 2015; Lynch et al., 2017). OPA1 is a dynamin-like GTPase which regulates the critical balance between fusion and fission in the dynamic mitochondrial network (MacVicar & Langer, 2016). Fission (division of a single organelle into two or more independent structures) and the opposing reaction (fusion) are the main processes for adapting mitochondrial morphology to metabolic changes and cellular needs (Lee & Yoon, 2016). They are governed by dynamin-related protein-1 (DRP1) for fission, and mitofusins (MFN1 and MFN2) and OPA1 for fusion of the outer mitochondrial membrane and inner membrane, respectively. OPA1 exists in eight different forms generated by alternative splicing and protease cleavage, which are usually seen as five bands in gels: two long forms (L1 and L2) and three short forms (S1-3) (Ishihara et al., 2006). Since balance between long (profusion) and short (profission) forms is required for the maintenance of mitochondrial morphology and fitness, OPA1 processing involves several mitochondrial proteases and is differentially regulated under stress conditions (Song

et al., 2007; Ehses et al., 2009; MacVicar & Langer, 2016). Interestingly, in the patient's cells, we observed a reduction of the long fusogenic OPA1 forms and an accumulation of the shortest ones that promote mitochondrial fission (Fig. 4B). Consistently, we observed fragmentation of the mitochondrial network which was present neither in SCA28 cells (Fig. 4C-D and Supp. Fig. S9) nor in SPG7 (paraplegin-deficient) cells (Pfeffer et al., 2014). Richter and coll. (Richter et al., 2015) proposed that the loss of *m*-AAA may lead to overaccumulation of *de novo* mito-synthesysed proteins in the IMM which in turn would cause mitochondrial membrane potential dissipation and activation of the OMA1 metalloprotease that processes the long OPA1 isoforms to the shortest ones. However, we could not detect any significant alteration of OMA1 mRNA in the patient's cells (Supp. Fig. S10), which suggests that activation, if any, of OMA1 occurs at the protein level, as previously proposed (Head et al., 2009; Baker et al., 2014; Bohovych et al., 2014; Consolato et al., 2018). We can therefore hypothesize that the simultaneous occurrence of an AFG3L2 dominant-negative mutation in the crucial ATP sensor and a halved dose of its companion paraplegin may alter both quantitatively and qualitatively the subunit composition and availability of *m*-AAA complexes to such extent as to severely impair mitochondria fitness with deficiency of respiratory chain Complex I and abnormal OPA1 processing by the stress-activated OMA1 protease, detectable also in non-neuronal cell lines. Furthermore, since expression data indicate that the levels of each subunit of the *m*-AAA protease are very different in distinct subsets of neurons (Martinelli et al., 2009; Di Bella et al., 2010), it is conceivable that a combined defect of both subunits might cause neuronal dysfunction distinct from that occurring in AFG3L2-associated SCA28 or paraplegin-associated SPG7, thus accounting for the peculiar phenotype observed in the patient reported here.

In conclusion, this study suggests that co-occurring mutations in both components of the mitochondrial *m*-AAA proteases may cause a novel *m*-AAA-pathy with a crucial pathogenic role of OPA1. These results would also widen the repertoire of disease genes causing early-onset parkinsonism and strengthen the crucial role of mitochondrial dysfunction — and in particular of mitochondrial dynamics and protein quality control — in a growing spectrum of neurodegenerative phenotypes. However, further experiments aimed at rescueing the cell phenotype and/or evidence for further cases with a similar genotype will be required for confirming that concurrent alterations of both components of the *m*-AAA complex are responsible for such a distinct cellular and clinical phenotype.

ACKNOWLEDGMENTS

We thank the patient and her family for participating in this study. We are grateful to Prof. Silvia De Biasi (University of Milan) for her help in confocal microscopy.

FUNDING

This work was supported by grants from the Italian Ministry of Health (RF-2011-02351165), E-Rare (E-Rare-2 JTC 2011 EuroSCAR), and Fondazione Telethon (GGP09301) to F.T.

DISCLOSURE STATEMENT

The authors have no conflict of interest to declare.

REFERENCES

Augustin, S., Gerdes, F., Lee, S., Tsai, F.T., Langer, T., & Tatsuta, T. (2009). An intersubunit signaling network coordinates ATP hydrolysis by m-AAA proteases. *Mol Cell*, *35*(5), 574-585.

Baker, M.J., Lampe, P.A., Stojanovski, D., Korwitz, A., Anand, R., Tatsuta, T., … Langer, T. (2014). Stress-induced OMA1 activation and autocatalytic turnover regulate OPA1-dependent mitochondrial dynamics. *EMBO J*, *33*(6), 578-593.

Bohovych, I., Donaldson, G., Christianson, S., Zahayko, N., & Khalimonchuk, O. (2014). Stress-triggered activation of the metalloprotease Oma1 involves its C-terminal region and is important for mitochondrial stress protection in yeast. *J Biol Chem*, *289*(19), 13259-13272.

Bonn, F., Tatsuta, T., Petrungaro, C., Riemer, J., & Langer, T. (2011). Presequence-dependent folding ensures MrpL32 processing by the *m*-AAA protease in mitochondria. *EMBO J*, *30*(13), 2545-2556.

Cagnoli, C., Mariotti, C., Taroni, F., Seri, M., Brussino, A., Michielotto, C., … Brusco, A. (2006). SCA28, a novel form of autosomal dominant cerebellar ataxia on chromosome 18p11.22-q11.2. *Brain*, *129*(Pt 1), 235-242.

Cagnoli, C., Stevanin, G., Brussino, A., Barberis, M., Mancini, C., Margolis, R.L., … Brusco, A. (2010). Missense mutations in the AFG3L2 proteolytic domain account for approximately 1.5% of European autosomal dominant cerebellar ataxias. *Hum Mutat*, *31*(10), 1117-1124.

Carelli, V., Musumeci, O., Caporali, L., Zanna, C., La Morgia, C., Del Dotto, V., … Zeviani, M. (2015). Syndromic parkinsonism and dementia associated with *OPA1* missense mutations. *Ann Neurol*, *78*(1), 21-38.

Casari, G., De Fusco, M., Ciarmatori, S., Zeviani, M., Mora, M., Fernandez, P., … Ballabio, A. (1998). Spastic paraplegia and OXPHOS impairment caused by mutations in paraplegin, a nuclear-encoded mitochondrial metalloprotease. *Cell*, *93*(6), 973-983.

Charif, M., Roubertie, A., Salime, S., Mamouni, S., Goizet, C., Hamel, C.P., … Lenaers, G. (2015). A novel mutation of *AFG3L2* might cause dominant optic atrophy in patients with mild intellectual disability. *Front Genet*, *6*311. doi: 10.3389/fgene.2015.00311. eCollection 2015.

Colavito, D., Maritan, V., Suppiej, A., Del Giudice, E., Mazzarolo, M., Miotto, S., … Leon, A. (2017). Non‐syndromic isolated dominant optic atrophy caused by the p.R468C mutation in the AFG3 like matrix AAA peptidase subunit 2 gene. *Biomed Rep*, *7*(5), 451-454.

Consolato, F., Maltecca, F., Tulli, S., Sambri, I., & Casari, G. (2018). m-AAA and i-AAA complexes coordinate to regulate OMA1, the stress-activated supervisor of mitochondrial dynamics. *J Cell Sci*, *131*(7),

Deka, R., Chakraborty, R., DeCroo, S., Rothhammer, F., Barton, S.A., & Ferrell, R.E. (1992). Characteristics of polymorphism at a VNTR locus 3’ to the apolipoprotein B gene in five human populations. *Am J Hum Genet*, *51*(6), 1325-1333.

Del Dotto, V., Mishra, P., Vidoni, S., Fogazza, M., Maresca, A., Caporali, L., … Zanna, C. (2017). OPA1 isoforms in the hierarchical organization of mitochondrial functions. *Cell Rep*, *19*(12), 2557-2571.

Di Bella, D., Lazzaro, F., Brusco, A., Plumari, M., Battaglia, G., Pastore, A., … Taroni, F. (2010). Mutations in the mitochondrial protease gene *AFG3L2* cause dominant hereditary ataxia SCA28. *Nat Genet*, *42*(4), 313-321.

Ehses, S., Raschke, I., Mancuso, G., Bernacchia, A., Geimer, S., Tondera, D., … Langer, T. (2009). Regulation of OPA1 processing and mitochondrial fusion by *m*-AAA protease isoenzymes and OMA1. *J Cell Biol*, *187*(7), 1023-1036.

Esser, K., Tursun, B., Ingenhoven, M., Michaelis, G., & Pratje, E. (2002). A novel two-step mechanism for removal of a mitochondrial signal sequence involves the *m*AAA complex and the putative rhomboid protease Pcp1. *J Mol Biol*, *323*(5), 835-843.

Eubanks, J.H., Selleri, L., Hart, R., Rosette, C., & Evans, G.A. (1991). Isolation, localization, and physical mapping of a highly polymorphic locus on human chromosome 11q13. *Genomics*, *11*(11), 720-729.

Ferreirinha, F., Quattrini, A., Pirozzi, M., Valsecchi, V., Dina, G., Broccoli, V., … Rugarli, E.I. (2004). Axonal degeneration in paraplegin-deficient mice is associated with abnormal mitochondria and impairment of axonal transport. *J Clin Invest*, *113*(2), 231-242.

Fracasso, V., Lazzaro, F., & Muzi-Falconi, M. (2010). Co-immunoprecipitation of human mitochondrial proteases AFG3L2 and paraplegin heterologously expressed in yeast cells. *Nat Protoc published online*, *doi: 10.1038/nprot.2010.26*

Gellera, C., Castellotti, B., Mariotti, C., Mineri, R., Seveso, V., DiDonato, S., … Taroni, F. (2007). Frataxin gene point mutations in Italian Friedreich ataxia patients. *Neurogenetics*, *8*(4), 289-299.

Head, B., Griparic, L., Amiri, M., Gandre-Babbe, S., & van der Bliek, A.M. (2009). Inducible proteolytic inactivation of OPA1 mediated by the OMA1 protease in mammalian cells. *J Cell Biol*, *187*(7), 959-966.

Ishihara, N., Fujita, Y., Oka, T., & Mihara, K. (2006). Regulation of mitochondrial morphology through proteolytic cleavage of OPA1. *EMBO J*, *25*(13), 2966-2977.

Klebe, S., Depienne, C., Gerber, S., Challe, G., Anheim, M., Charles, P., … Durr, A. (2012). Spastic paraplegia gene 7 in patients with spasticity and/or optic neuropathy. *Brain*, *135*(Pt 10), 2980-2993.

Koopman, W.J., Visch, H.J., Smeitink, J.A., & Willems, P.H. (2006). Simultaneous quantitative measurement and automated analysis of mitochondrial morphology, mass, potential, and motility in living human skin fibroblasts. *Cytometry A*, *69*(1), 1-12.

Koppen, M., Bonn, F., Ehses, S., & Langer, T. (2009). Autocatalytic processing of *m*-AAA protease subunits in mitochondria. *Mol Biol Cell*, *20*(19), 4216-4224.

Koppen, M., & Langer, T. (2007). Protein degradation within mitochondria: versatile activities of AAA proteases and other peptidases. *Crit Rev Biochem Mol Biol*, *42*(3), 221-242.

Lee, H., & Yoon, Y. (2016). Mitochondrial fission and fusion. *Biochem Soc Trans*, *44*(6), 1725-1735.

Lynch, D.S., Loh, S.H.Y., Harley, J., Noyce, A.J., Martins, L.M., Wood, N.W., … Plun-Favreau, H. (2017). Nonsyndromic Parkinson disease in a family with autosomal dominant optic atrophy due to *OPA1* mutations. *Neurol Genet*, *3*(5), e188.

MacVicar, T., & Langer, T. (2016). OPA1 processing in cell death and disease - the long and short of it. *J Cell Sci*, *129*(12), 2297-2306.

Magri, S., Fracasso, V., Rimoldi, M., & Taroni, F. (2010). Preparation of yeast mitochondria and *in vitro* assay of respiratory chain complex activities. *Nat Protoc published online*, *doi: 10.1038/nprot.2010.25*

Maltecca, F., Aghaie, A., Schroeder, D.G., Cassina, L., Taylor, B.A., Phillips, S.J., … Casari, G. (2008). The mitochondrial protease AFG3L2 is essential for axonal development. *J Neurosci*, *28*(11), 2827-2836.

Maltecca, F., Magnoni, R., Cerri, F., Cox, G.A., Quattrini, A., & Casari, G. (2009). Haploinsufficiency of AFG3L2, the gene responsible for spinocerebellar ataxia type 28, causes mitochondria-mediated Purkinje cell dark degeneration. *J Neurosci*, *29*(29), 9244-9254.

Martinelli, P., La Mattina, V., Bernacchia, A., Magnoni, R., Cerri, F., Cox, G., … Rugarli, E.I. (2009). Genetic interaction between the *m*-AAA protease isoenzymes reveals novel roles in cerebellar degeneration. *Hum Mol Genet*, *18*(11), 2001-2013.

Muona, M., Berkovic, S.F., Dibbens, L.M., Oliver, K.L., Maljevic, S., Bayly, M.A., … Lehesjoki, A.E. (2015). A recurrent de novo mutation in *KCNC1* causes progressive myoclonus epilepsy. *Nat Genet*, *47*(1), 39-46.

Muzi-Falconi, M., Piseri, A., Ferrari, M., Lucchini, G., Plevani, P., & Foiani, M. (1993). De novo synthesis of budding yeast DNA polymerase alpha and POL1 transcription at the G1/S boundary are not required for entrance into S phase. *Proc Natl Acad Sci U S A*, *90*(22), 10519-10523.

Nolden, M., Ehses, S., Koppen, M., Bernacchia, A., Rugarli, E.I., & Langer, T. (2005). The *m*-AAA protease defective in hereditary spastic paraplegia controls ribosome assembly in mitochondria. *Cell*, *123*(2), 277-289.

Ogura, T., Whiteheart, S.W., & Wilkinson, A.J. (2004). Conserved arginine residues implicated in ATP hydrolysis, nucleotide-sensing, and inter-subunit interactions in AAA and AAA+ ATPases. *J Struct Biol*, *146*(1-2), 106-112.

Palmfeldt, J., Vang, S., Stenbroen, V., Pedersen, C.B., Christensen, J.H., Bross, P., … Gregersen, N. (2009). Mitochondrial proteomics on human fibroblasts for identification of metabolic imbalance and cellular stress. *Proteome Sci*, *7*20 doi:10.1186/1477-5956.

Pfeffer, G., Gorman, G.S., Griffin, H., Kurzawa-Akanbi, M., Blakely, E.L., Wilson, I., … Chinnery, P.F. (2014). Mutations in the *SPG7* gene cause chronic progressive external ophthalmoplegia through disordered mitochondrial DNA maintenance. *Brain*, *137*(Pt 5), 1323-1336.

Pierson, T.M., Adams, D., Bonn, F., Martinelli, P., Cherukuri, P.F., Teer, J.K., … Toro, C. (2011). Whole-exome sequencing identifies homozygous *AFG3L2* mutations in a spastic ataxia-neuropathy syndrome linked to mitochondrial *m*-AAA proteases. *PLoS Genet*, *7*(10), e1002325.

Quirós, P.M., Ramsay, A.J., Sala, D., Fernández-Vizarra, E., Rodríguez, F., Peinado, J.R., … López-Otín, C. (2012). Loss of mitochondrial protease OMA1 alters processing of the GTPase OPA1 and causes obesity and defective thermogenesis in mice. *EMBO J*, *31*(9), 2117-2133.

Richards, S., Aziz, N., Bale, S., Bick, D., Das, S., Gastier-Foster, J., … ACMG, L.Q.A.C. (2015). Standards and guidelines for the interpretation of sequence variants: a joint consensus recommendation of the American College of Medical Genetics and Genomics and the Association for Molecular Pathology. *Genet Med*, *17*(5), 405-424.

Richter, U., Lahtinen, T., Marttinen, P., Suomi, F., & Battersby, B.J. (2015). Quality control of mitochondrial protein synthesis is required for membrane integrity and cell fitness. *J Cell Biol*, *211*(2), 373-389.

Song, Z., Chen, H., Fiket, M., Alexander, C., & Chan, D.C. (2007). OPA1 processing controls mitochondrial fusion and is regulated by mRNA splicing, membrane potential, and Yme1L. *J Cell Biol*, *178*(5), 749-755.

Suno, R., Niwa, H., Tsuchiya, D., Zhang, X., Yoshida, M., & Morikawa, K. (2006). Structure of the whole cytosolic region of ATP-dependent protease FtsH. *Mol Cell*, *22*(5), 575-585.

Tatsuta, T., Augustin, S., Nolden, M., Friedrichs, B., & Langer, T. (2007). *m*-AAA protease-driven membrane dislocation allows intramembrane cleavage by rhomboid in mitochondria. *EMBO J*, *26*(2), 325-335.

Veitia, R.A., Caburet, S., & Birchler, J.A. (2018). Mechanisms of Mendelian dominance. *Clin Genet*, *93*(3), 419-428.

Wong, A., Yang, J., Cavadini, P., Gellera, C., Lonnerdal, B., Taroni, F., … Cortopassi, G.A. (1999). The Friedreich's ataxia mutation confers cellular sensitivity to oxidant stress which is rescued by chelators of iron and calcium and inhibitors of apoptosis. *Hum Mol Genet*, *8*(3), 425-430.

Legends to figures

Figure 1. Segregation of *AFG3L2* and *SPG7* mutations and SPECT/DaTscan

(A) Pedigree of family MI-PPS0722. Square and circle symbols are male and female individuals, respectively. The symbol filled in black represents the affected individual. *AFG3L2* and *SPG7* genotypes are indicated under the symbols of the sampled individuals. Non-paternity for subject I-1 could be confidently excluded by segregation analyis using highly polymorphic VNTR markers (3'APOB-VNTR and D11S533). Low-level somatic mosaicism for *AFG3L2*^{R468C} was also excluded by deep sequencing for both I-1 and I-2 (see

Supp. Fig. S4). **(B)** Single photon emission computed tomography (SPECT) brain imaging with ^{123}I-Ioflupane injection (DaTscan™) in the proband II-1. Semi-quantitative analysis showed bilateral depletion of striatal dopamine transporter. Striatum: 0.65 (R), 0.67 (L) (*n.v.*, 1.5-2.9); caudate: 0.75 (R), 0.78 (L) (*n.v.*, 1.7-3.3); putamen: 0.52 (R), 0.56 (L) (*n.v.*, 1.4-3.1); putamen/caudate ratio: 0.70 (R), 0.71 (L) (*n.v.*, ≥0.7).

A

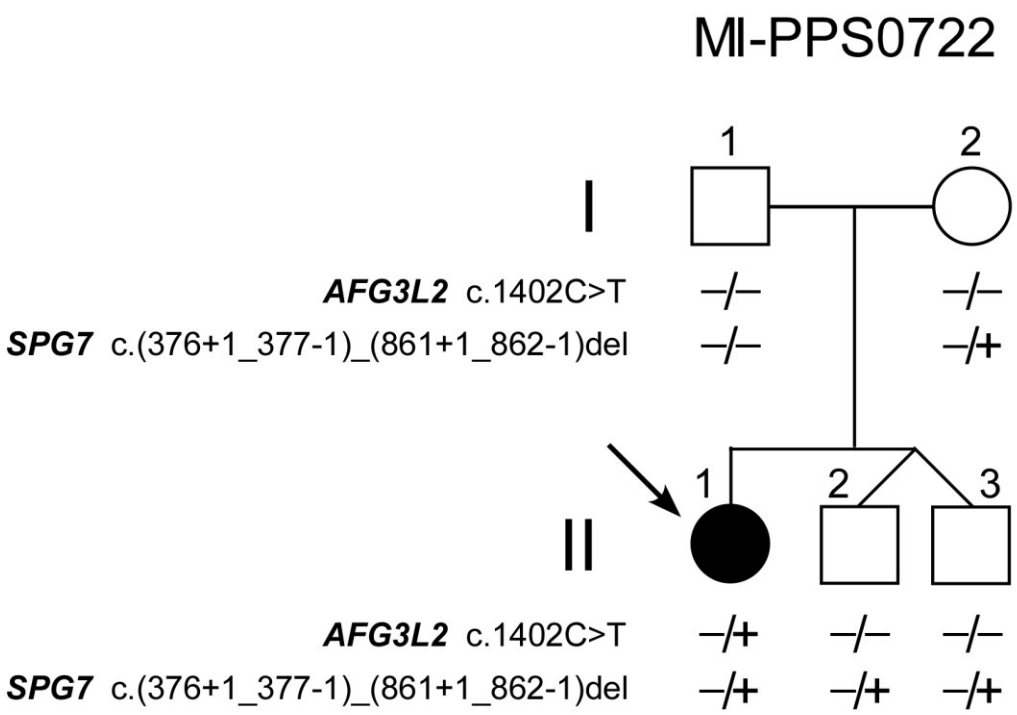

B

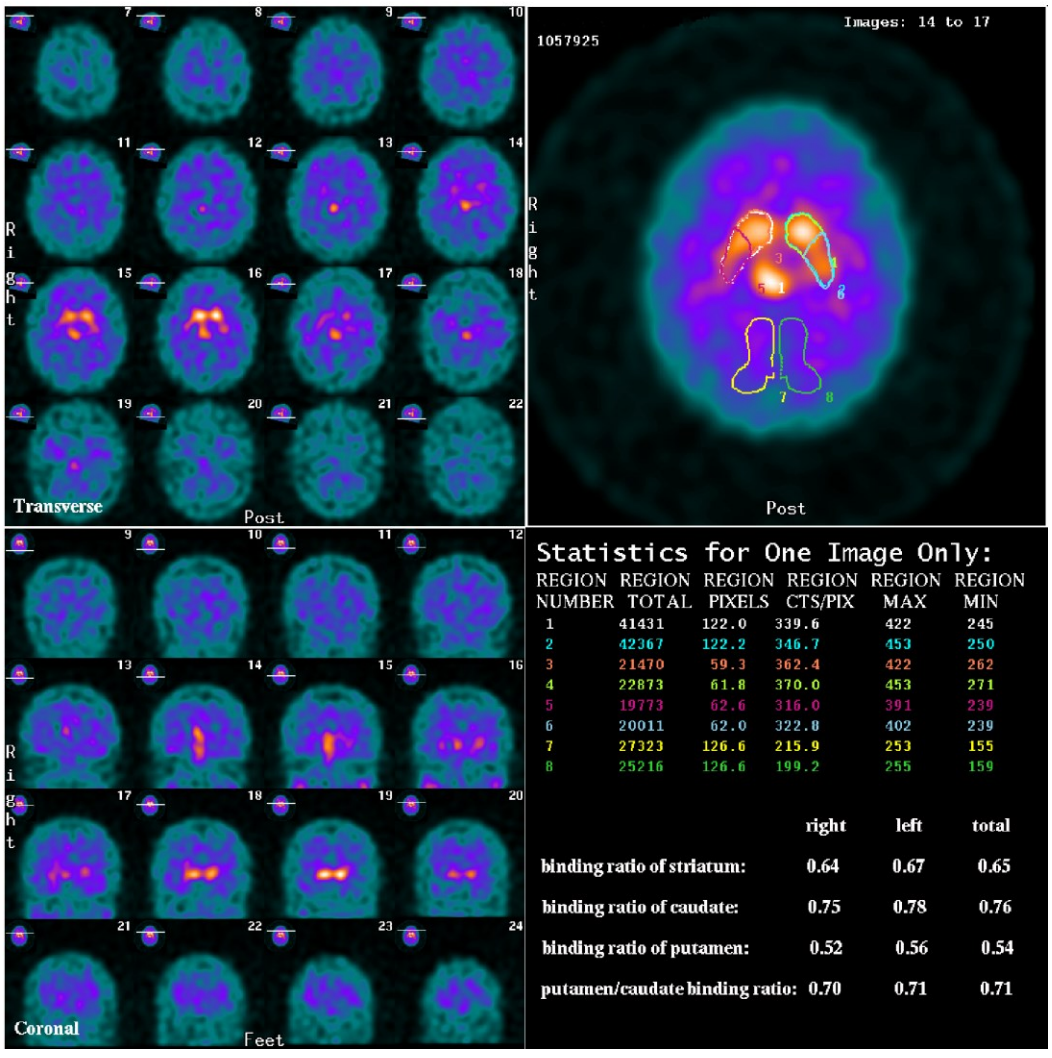

Figure 2. Respiratory phenotype of *yta10*Δ*yta12*Δ yeast cells expressing AFG3L2^{R468C}

(A, B) Serial dilutions of normalized yeast cultures were spotted on YEP plates containing 2% glucose (YPD) or 2% glycerol (YPG) and incubated at 28°C for 3 days. Respiratory competence was deduced by the ability to grow on 2% glycerol (YPG). **(A)** Respiratory phenotype of K699 (WT yeast strain) and *yta10*Δ*yta12*Δ cells expressing either normal (WT) or mutant human AFG3L2 (p.R468C and the two reference mutations p.E691K and p.S674L previously described (Di Bella et al., 2010)). **(B)** Respiratory phenotype of K699 and *yta10*Δ*yta12*Δ cells coexpressing either normal or mutant human AFG3L2 with human paraplegin. **(C)** Enzyme activity of respiratory chain complexes III, IV, and V in isolated mitochondria from *yta10*Δ*yta12*Δ *m*-AAA-deficient yeast cells expressing normal or mutated AFG3L2 in the absence and in the presence of paraplegin. Ubiquinol *c* oxidoreductase (Complex III) specific activity is expressed as nanomoles of cytochrome *c* reduced per minute per milligram of protein. Cytochrome *c* oxidase (Complex IV) specific activity is expressed as nanomoles of cytochrome c^{red} oxidized per minute per milligram of protein. ATPase (Complex V) specific activity is expressed as nanomoles of NADH oxidized per minute per milligram of protein. Bars and vertical lines indicate mean and ±1SD of 3 independent experiments, respectively. Values in parentheses indicate percentage of activity compared to that of AFG3L2^{WT}. Asterisks indicate a statistically significant (*$P \leq 0.05$; **$P \leq 0.005$) difference from AFG3L2^{WT}, as determined by Student's *t*-test.

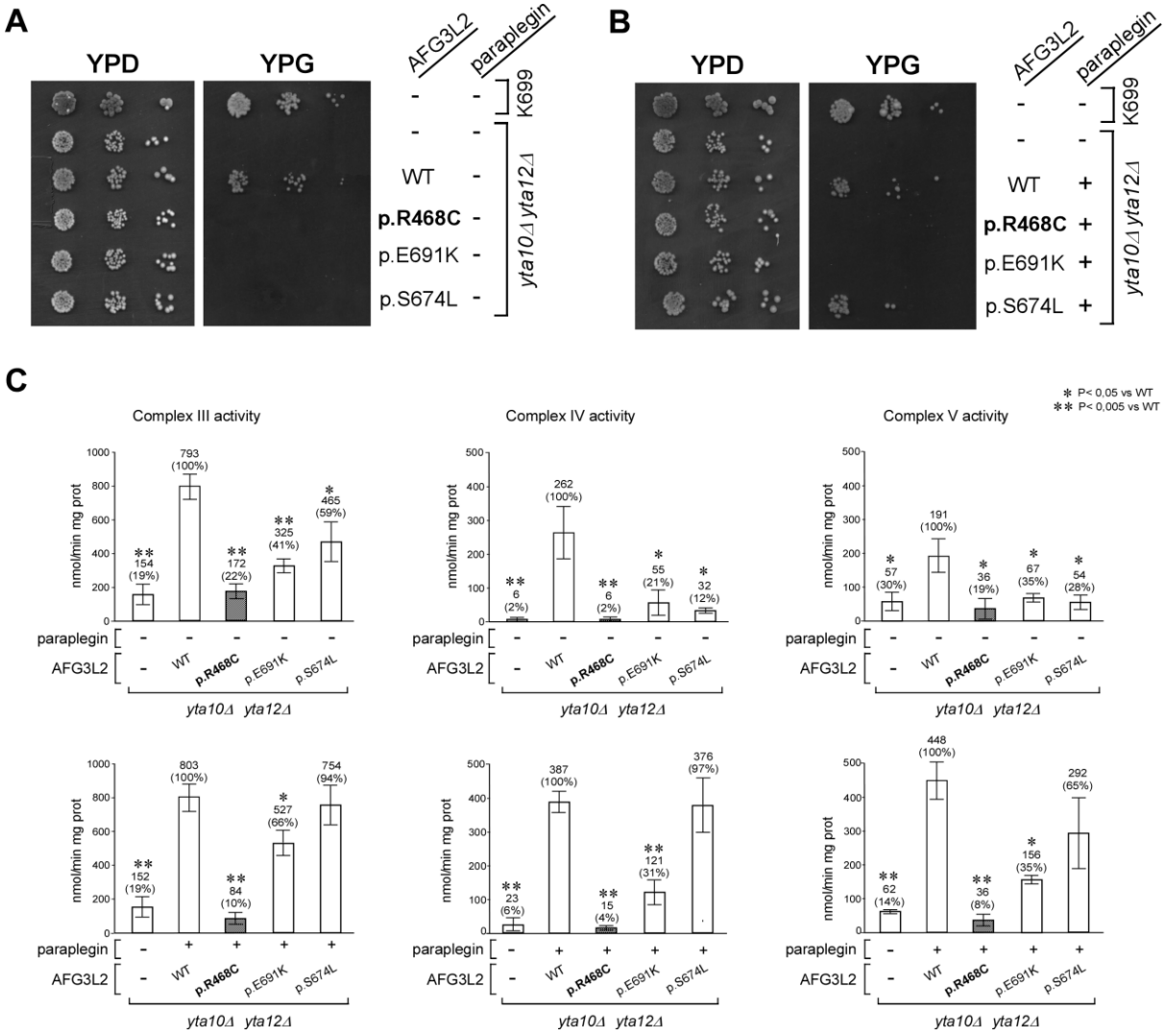

Figure 3. Functional analysis of *m*-AAA in yeast

(A, B) Proteolytic and dislocase (ATPase) activity of AFG3L2^{R468C} in yeast. **(A)** Fluorescence immunoblot analysis of MrpL32 precursor (p) and mature (m) form in yeast cells expressing either WT or mutant human AFG3L2 (left panel) and co-expressed with paraplegin (right panel). Proteolytic competence is measured as precursor accumulation expressed as the percent ratio of precursor level to total (p + m) level. MrpL32 levels were normalized to the loading control protein β-actin. Histograph reports densitometric quantitation of precursor accumulation (indicated by p/(p + m) %) of 3 independent

experiments. Asterisks indicate a statistically significant (*$P \leq 0.01$; **$P \leq 0.001$) difference from AFG3L2^{WT} (lane 2) as determined by Student's *t*-test. **(B)** Fluorescence immunoblot analysis of Ccp1 precursor (p) and mature (m) forms in yeast cells expressing either WT or mutant human AFG3L2 (left panel) and coexpressed with paraplegin (right panel). The dislocase (ATPase) competence is measured as precursor accumulation expressed as the percent ratio of precursor level to total (p + m) level. Ccp1 levels were normalized to the loading control protein β-actin. Each bar graph reports densitometric quantification of precursor accumulation (indicated by p/(p + m) %) of 3 independent experiments. Asterisks indicate a statistically significant (*$P \leq 0.05$; **$P \leq 0.0005$) difference from AFG3L2^{WT} (lane 2) as determined by Student's *t*-test. Red bars: strain expressing AFG3L2^{R468C}; blue bars: reference strains (*yta10*Δ*yta12*Δ, AFG3L2^{WT} and control mutants as in Fig. 2). Bars and vertical lines indicate mean and ±1SD, respectively. **(C, D)** *m*-AAA maturation impairment in yeast strain expressing AFG3L2^{R468C}. **(C)** Immunoblot analysis of human AFG3L2 autocatalytic processing in yeast strains. **(D)** Immunoblot analysis of human AFG3L2 autocatalytic processing and paraplegin maturation in strains coexpressing paraplegin. m, mature; p, precursor; i, intermediate. Asterisks indicate paraplegin nonspecific degradation products.

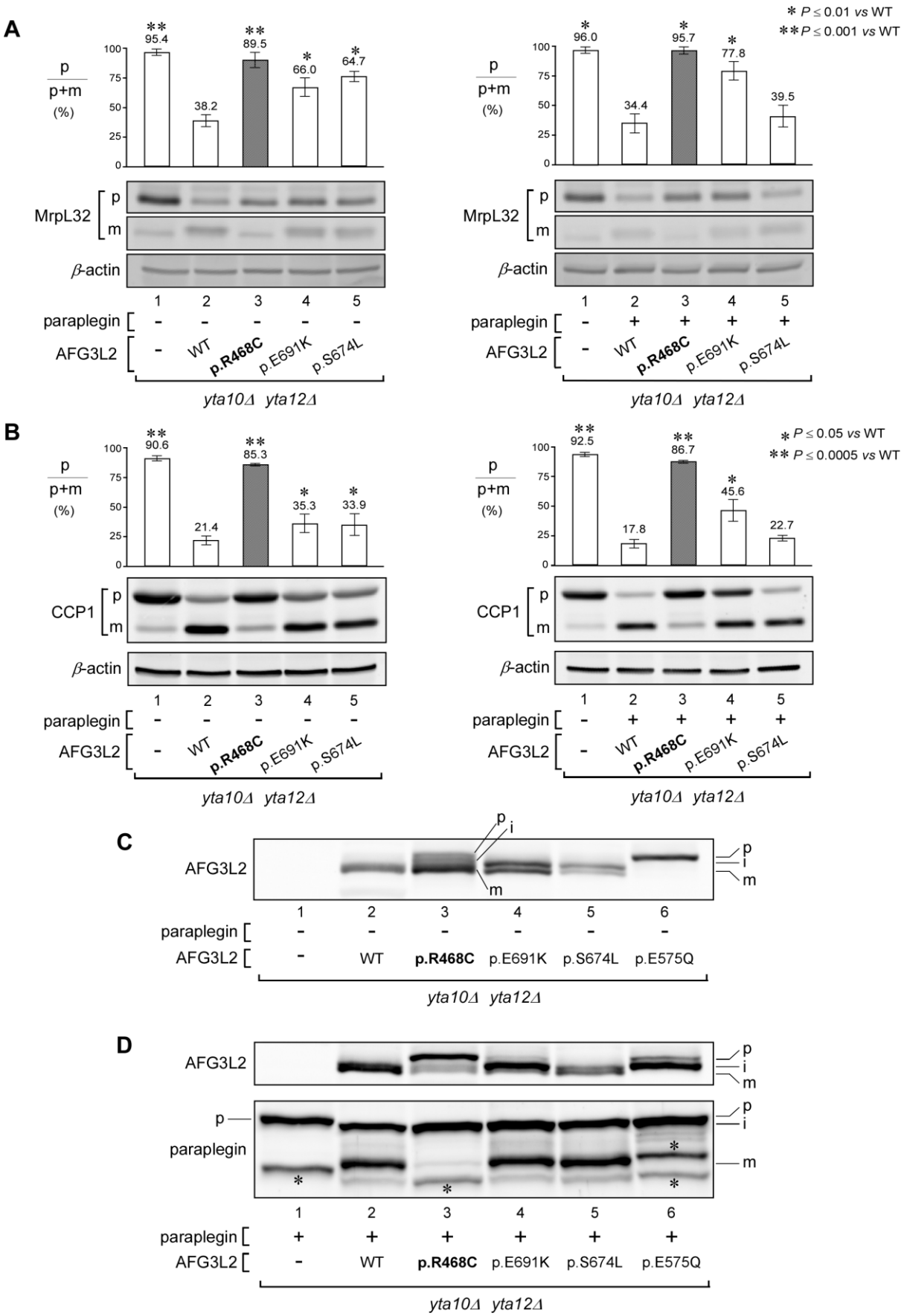

Figure 4. OPA1 and mitochondrial network analysis in patient's fibroblasts

(A) Immunoblot and quantitative analysis of OPA1 in fibroblast extracts cultured in medium containing glucose or galactose, a mild metabolic stress inducer that enhances mitochondrial dysfunction (Palmfeldt et al., 2009). The alpha subunit of mitochondrial trifunctional protein (MTPα) was used as a loading control. OPA1 long forms (L1 and L2) short forms (S1, S2 and S3). C1 and C2, normal controls; P, patient. Histograph reports densitometric quantitation of OPA1 forms (expressed as OPA1 form/total OPA1 %) of 3 independent experiments. Bars and vertical lines indicate means and ± 1 SD, respectively. **(B, C)** Analysis of mitochondrial morphology in patient-derived fibroblasts. **(B)** Representative confocal images of mitochondria stained with Mitotracker Red. Control and patient fibroblasts cultured in glucose or galactose medium were stained with Mitotracker Red. Scale bars = 5 μm. **(C)** The graph shows average Aspect ratio (shape) and Formfactor (branching) values for mitochondria in the four conditions: patients or control cells cultured with or without galactose. Bars and vertical lines indicate means and ± 1 SD, respectively, of values obtained from the analysis of four randomly selected cells. Red bars = patient; Blue bars = control. Asterisks indicate a statistically significant (*$P \leq 0.005$) difference from control as determined by Student's t-test. C, control, P, patient.